ORIGINAL RESEARCH

Graphene Oxide Quantum Dots-Preactivated Dental Pulp Stem Cells/GelMA Facilitates Mitophagy-Regulated Bone Regeneration

Xiaoyuan Yan[1], Na An[2], Zeying Zhang[1], Qiujing Qiu ⓘ[1], Di Yang[1], Penggong Wei[1], Xiyue Zhang[1], Lihong Qiu[1], Jiajie Guo[1]

[1]Department of Endodontics, School and Hospital of Stomatology, China Medical University, Liaoning Provincial Key Laboratory of Oral Diseases, Shenyang, People's Republic of China; [2]Department of Orthodontics, School and Hospital of Stomatology, China Medical University, Liaoning Provincial Key Laboratory of Oral Diseases, Shenyang, People's Republic of China

Correspondence: Lihong Qiu; Jiajie Guo, Department of Endodontics, School and Hospital of Stomatology, China Medical University, Liaoning Provincial Key Laboratory of Oral Diseases, No. 117 Nanjing North Street, Heping District, Shenyang, Liaoning Province, People's Republic of China, Email lhqiu@cmu.edu.cn; guojiajie@cmu.edu.cn

Background: In bone tissue engineering (BTE), cell-laden scaffolds offer a promising strategy for repairing bone defects, particularly when host cell regeneration is insufficient due to age or disease. Exogenous stem cell-based BTE requires bioactive factors to activate these cells. Graphene oxide quantum dots (GOQDs), zero-dimensional derivatives of graphene oxide, have emerged as potential osteogenic nanomedicines. However, constructing biological scaffolds with GOQDs and elucidating their biological mechanisms remain critical challenges.

Methods: We utilized GOQDs with a particle size of 10 nm, characterized by a surface rich in C–O–H and C–O–C functional groups. We developed a gelatin methacryloyl (GelMA) hydrogel incorporated with GOQDs-treated dental pulp stem cells (DPSCs). These constructs were transplanted into rat calvarial bone defects to estimate the effectiveness of GOQDs-induced DPSCs in repairing bone defects while also investigating the molecular mechanism underlying GOQDs-induced osteogenesis in DPSCs.

Results: GOQDs at 5 μg/mL significantly enhanced the osteogenic differentiation of DPSCs without toxicity. The GOQDs-induced DPSCs showed active osteogenic potential in three-dimensional cell culture system. In vivo, transplantation of GOQDs-preactivated DPSCs/GelMA composite effectively facilitated calvarial bone regeneration. Mechanistically, GOQDs stimulated mitophagy flux through the phosphatase-and-tensin homolog-induced putative kinase 1 (PINK1)/Parkin E3 ubiquitin ligase (PRKN) pathway. Notably, inhibiting mitophagy with cyclosporin A prevented the osteogenic activity of GOQDs.

Conclusion: This research presents a well-designed bionic GOQDs/DPSCs/GelMA composite scaffold and demonstrated its ability to promote bone regeneration by enhancing mitophagy. These findings highlight the significant potential of this composite for application in BTE and underscore the crucial role of mitophagy in promoting the osteogenic differentiation of GOQDs-induced stem cells.

Keywords: graphene oxide quantum dots, dental pulp stem cells, osteogenesis, bone regeneration, mitophagy

Introduction

Bone tissue engineering (BTE) has emerged as a promising approach for treating bone defects, utilizing biomimetic substitutes composed of seed cells, bioactive factors and scaffolds.[1] Compared with acellular scaffolds, cell-laden scaffolds demonstrate greater therapeutic potential for repairing bone defects, particularly in patients with insufficient host cell regeneration due to age, disease, or other factors. Dental pulp stem cells (DPSCs) are mesenchymal stem cells (MSCs) found in dental pulp tissue, characterized by their multidirectional differentiation potential. They can differentiate into odontoblasts, osteoblasts, chondroblasts, adipocytes, and neuronal cells in vitro after drug induction.[2,3] A significant number of intact wisdom teeth and teeth extracted for orthodontic reduction can serve as sources of DPSCs. This abundance of DPSCs provides an advantage over bone marrow stem cells (BMSCs), which are the traditional seed

cells used in BTE, as their acquisition does not entail additional trauma or pain for patients. Since the differentiation efficiency of exogenous stem cells at the recipient site may be limited by the host microenvironment, bioactive factors that promote differentiation become increasingly important. However, the most commonly used bioactive factors in BTE, bone morphogenetic proteins (BMPs), are expensive and can lead to clinical side effects, including ectopic bone and arthritis.[4–6] Consequently, new bone regeneration medicines that are safe and effective are still needed.

Graphene oxide quantum dots (GOQDs) are a type of zero-dimensional carbon nanomaterial with a lateral size less than 20 nm.[7] Although GOQDs are derivatives of graphene oxide (GO), they are smaller, more biocompatible, and can be cleared from the body more rapidly than GO.[8,9] Additionally, GOQDs possess active chemical properties due to the abundant oxygenated functional groups on their surfaces.[10] Initially developed as a class of semiconductors for use in batteries and electronic devices, GOQDs have recently garnered attention from biomedical researchers as promising nanomedicines for bone regeneration.[11–15] One study demonstrated that coating metal implants with GOQDs enhanced the repair of bone defects in rabbit femurs.[12] Furthermore, in vitro studies have indicated that GOQDs promote the osteogenic differentiation of BMSCs by activating the Wnt/β-catenin pathway.[12] Li et al found that GOQDs induced DPSCs to differentiate into osteoblasts through reactive oxygen species-dependent autophagy pathway.[13] Additionally, Yang's team revealed that GOQDs facilitated the osteogenic differentiation of stem cells from human exfoliated deciduous teeth (SHEDs) via elevating Wnt/β-catenin signaling.[14,15] These studies suggest the potential application of GOQDs as bioactive factors for promoting bone defect repair. However, the in vivo osteogenic activity of GOQDs, particularly in conjunction with DPSCs for the repair of bone defects, remains to be investigated. The optical methods for constructing GOQDs, stem cells and scaffolds have not been completely defined. Moreover, the molecular mechanisms by which GOQDs promote the osteogenic differentiation of stem cells are also not well understood. These research gaps have limited the advancement of GOQDs in BTE. Given that bone defects can vary significantly in shape and size, malleable scaffolds are essential for use in BTE. Gelatin methacryloyl (GelMA) is a biocompatible and biodegradable hydrogel with excellent plasticity, making it suitable for adapting to the different shapes and sizes of bone defects.[16,17] Therefore, this study aims to optimize the combination of GOQDs, DPSCs, and GelMA scaffolds, and to evaluate whether this construct can safely and effectively repair bone defects in vivo.

The utilization of GOQDs in BTE is impeded by the insufficient understanding of the mechanisms by which GOQDs promote the osteogenic differentiation of MSCs; thus, exploring these molecular mechanisms is of paramount importance. The process of encapsulating damaged mitochondria into autophagosomes for subsequent degradation in lysosomes, known as mitophagy, is essential for maintaining mitochondrial quality and ensuring a reliable energy supply during cell growth and differentiation.[18] Previous studies have indicated that while graphene and GO are primarily entrapped within lysosomes upon cellular internalization, a small fraction of graphene interact with mitochondria.[19,20] However, there is a notable lack of research investigating whether GOQDs affect mitophagy flux in DPSCs or whether mitophagy plays a role in the GOQDs-induced osteogenesis of MSCs.

In this study, we evaluated the effect of GOQDs on the osteogenic differentiation of DPSCs in vitro. We subsequently constructed a biomimetic substitute comprising GOQDs, DPSCs, GelMA and investigated its efficacy in repairing rat calvarial bone defects. Furthermore, we explored whether GOQDs promote the osteogenic differentiation of DPSCs by regulating mitophagy. Our findings demonstrated the osteogenic effects of GOQDs and elucidated the underlying mechanism in detail, suggesting that GOQDs have potential applications in BTE; in addition, these results contributed to the knowledge on the osteogenic function of GOQDs and the cellular response to GOQDs.

Materials and Methods
Isolation and Culture of Human Primary DPSCs
This study was reviewed and approved by the Medical Ethics Committee of the School of Stomatology, China Medical University (Grant No. 2018009). All the experimental procedures were in accordance with The Code of Ethics of the World Medical Association (Declaration of Helsinki). Isolated teeth that were extracted due to obstruction and the need for orthodontic reduction were collected. The inclusion criteria for isolated teeth were as follows: (1) the patient was 18–25 years of age, (2) the apical foramen was closed, (3) the patient had no systemic disease, and (4) the dentition and

periodontal tissues were intact. All patients provided informed consent. The pulp was removed from the teeth and transferred to a mixture (1:1) of type I collagenase (3 mg/mL; Sigma–Aldrich, USA) and dispase (4 mg/mL; Solarbio, China), where it was well sheared and subsequently digested at 37 °C for 5 to 15 min. The enzyme solution was subsequently discarded. Next, the pulp tissues were cultured in α-MEM (Gibco, USA) supplemented with 20% fetal bovine serum (FBS; Clark, USA), 100 units/mL penicillin and 100 g/mL streptomycin (HyClone, USA). Half of the medium was changed after 7 days, and the full amount was changed after 10 days. Cells were passaged when their density reached 80%, and the passaged cells were cultured in α-MEM supplemented with 10% FBS (complete medium, CM). The 3rd–6th generation of cells was used for the subsequent experiments.

Characterization of GOQDs

GOQDs dispersion (1 mg/mL; XF074-1) was purchased from Nanjing XFNANO Materials Tech Co., Ltd (China). A high-resolution field emission transmission electron microscope (HRTEM; JEOL, Japan) was used to photograph and observe the dispersion of GOQDs in water, and the particle size of GOQDs was measured and counted using Nanomeasure software. Atomic force microscopy (AFM; SHIMADZU, Japan) was used to photograph the dispersion of GOQDs, and the height of the quantum dots was analyzed using Gwyddion software. The photoluminescence (PL) spectra of GOQDs were detected using excitation light in a wavelength range from 350 to 500 nm. For X-ray photoelectron spectroscopy (XPS) analysis, the GOQDs dispersion samples were coated on a silicon substrate, dried, glued to the sample stage, and subsequently analyzed via an XPS analyzer (Thermo Fisher, USA) for full-spectrum analysis and fine-spectral analysis of carbon and oxygen after vacuuming.

Flow Cytometry

A total of 1×10^6 cells (100 μL) were pipetted into each of the six tubes. The first tube contained a blank group without any antibody, and the other five tubes contained 5 μL of phycoerythrin (PE) -conjugated anti-CD14, anti-CD29, anti-CD45, anti-CD105 or anti-CD146 (Biolegend, USA). After incubating for 20 min at room temperature, the cells were washed twice with PBS containing 3% FBS and centrifuged at 1000 rpm for 4 min. Then, 0.5 mL of PBS containing 3% FBS was added to each tube to resuspend the cells, and flow cytometry was performed via a flow cytometer (BD, USA).

Induction of Adipogenic Differentiation and Oil Red O Staining

The adipogenic induction solutions included solution A and solution B. Solution A was high-glucose DMEM containing 0.2 mm indomethacin (Aladdin, China), 10 μg/mL insulin (Solarbio, China), 0.5 mm 3-isobutyl-1-methylxanthine (IBMX, Aladdin, China), and 1 μM dexamethasone. Solution B was high-glucose DMEM containing 10 μg/mL insulin. The cells were induced with solution A for three days and then with solution B for one day, and the cycle was repeated 5 times. On day 21, Oil Red O staining was performed according to the instructions of the Modified Oil Red O Staining Kit (Beyotime, China) to examine the droplets within the cells.

Induction of Chondrogenic Differentiation and Alcian Blue Staining

Chondrogenic induction and alcian blue staining were performed according to instructions of the OriCell® Human Related Stem Cells Chondrogenic Differentiation Induction Kit (Cyagen, China).

Induction of Osteogenic Differentiation

To characterize the osteogenic differentiation ability of the cells, they were incubated with growth medium (GM) or osteogenic medium (OM), and the GM group served as the control. GM was high-glucose DMEM (BioInd, Israel) supplemented with 10% FBS. OM was high-glucose DMEM supplemented with 10% FBS, 100 nM dexamethasone, 10 μM β-glycerophosphate disodium salt hydrate (Sigma–Aldrich, USA) and 50 μg/mL L-ascorbic acid (Sigma–Aldrich, USA). To determine the osteogenic activity of GOQDs, cells were cultured with OM or OM containing GOQDs, and OM group served as the control. The medium was changed every 2 days.

Alkaline Phosphatase (ALP) Staining and Activity Assay

For the ALP staining assay, DPSCs were seeded in twelve-well plates at 7×10^4 cells per well. ALP staining was performed after osteogenic differentiation was induced for 8 days. The cells were fixed with 4% paraformaldehyde at room temperature for 10 min and then washed with PBS. Subsequent staining was performed according to instructions of the BCIP/NBT ALP Color Development Kit (Beyotime, China). An ALP activity quantitative assay was also performed according to instructions of the Alkaline Phosphatase Assay Kit (Beyotime, China) after osteoblastic differentiation was induced for 8 days.

Alizarin Red S (ARS) Staining and Quantification of Mineralized Nodules

Five hundred milligrams of ARS powder (Sigma–Aldrich, USA) was dissolved in 50 mL of deionized water, and the pH was adjusted to 6.4. ARS staining was performed after osteogenic differentiation was induced for 21 days. The cells were fixed with 4% paraformaldehyde for 10 min at room temperature and subsequently with 95% ethanol under the same conditions for 10 min. Next, the cells were stained with ARS staining solution at room temperature for 10 min and subsequently washed twice with deionized water. For the quantification of mineralized nodules, 10% (w/v) hexadecyl-pyridinium chloride (Aladdin, China) was dissolved in PBS (pH = 7.0). The ARS-stained plates were air-dried, and 1 mL of hexadecylpyridinium chloride solution was added to dissolve the mineralized nodules for 15 min. The dissolution solution was added to 96-well plates, with three replicate wells in each group and 100 µL in each well; the absorbance at 540 nm was detected by a microplate reader (Tecan, Switzerland).

Cell Viability Assay

Cells (5×10^3/well) were inoculated in 96-well plates with 200 µL of GM at 37 °C. After 24 h, the medium was replaced with 200 µL of fresh GM with or without GOQDs. The culture medium was changed every three days. Cell viability was determined by CKK-8 according to instructions of the Cell Counting Kit-8 (APEXBIO, USA) at the indicated time points.

Western Blot (WB)

The cells were lysed with Cell Lysis Buffer (Beyotime, China) and sonicated. The protein concentration was determined using the Detergent Compatible Bradford Protein Assay Kit (Beyotime, China). Denatured proteins were separated by SDS-PAGE (Epizyme, China) and then transferred to nitrocellulose membranes (PALL, USA). After blocking with 5% (w/v) nonfat milk (Beyotime, China) for 1 h, the membranes were incubated with antibodies at 4 °C overnight and then with secondary antibodies (Proteintech, China) at room temperature for 1 h. The signal intensity was detected with an Odyssey® DLx imaging system (LI-COR, USA). Fiji software was used to quantify the band intensities. The antibodies used in the present study are as follows: osteogenic markers including Collagen Type I (Col-1; Proteintech, China), Osteopontin (OPN; ABclonal, China), Runt-related transcription factor 2 (Runx2; CST, USA) and Osterix (Osx; Abcam, USA); mitophagy markers including phosphatase-and-tensin homolog-induced putative kinase 1 (PINK1; CST, USA), Parkin E3 ubiquitin ligase (PRKN; CST, USA), p62 (CST, USA), and LC3 (ABclonal, China); and Glyceraldehyde-3-phosphate dehydrogenase (GAPDH; Affinity, China).

Scratch Experiment

The cells were inoculated into a six-well plate (1.1×10^6/well), and scratches were created with a 20 µL pipette tip 24 h after the cells had been incubated in GM. After washed with PBS to remove floating cells, the cells were then incubated in low-serum medium (α-MEM containing 2% FBS) alone or with different concentrations of GOQDs (1, 5, 10, or 20 µg/mL) and photographed using a microscope 3 h and 24 h later. The scratch width at two time points was measured using ImageJ software. The migration distance was obtained by subtracting the scratch width at 24 h from that at 3h. The migration index was obtained by dividing the migration distance of the experimental groups by that of the control group (0 µg/mL group).

Vitro Growth and Differentiation Capacity of DPSCs in GelMA

The lyophilized GelMA used in this study was purchased from EFL Co., Ltd. (China). For 6% GelMA, 0.6 g of lyophilized GelMA was dissolved in 10 mL of PBS; for 9% GelMA, 0.9 g of lyophilized GelMA was dissolved in 10 mL of PBS; and for 12% GelMA, 1.2 g of lyophilized GelMA was dissolved in 10 mL PBS. Lyophilized GelMA was dissolved in PBS in 65 °C for approximately 10 min and to obtain a GelMA hydrogel precursor solution.

To obtain GelMA constructs, 0.2 mL of 6%, 9% or 12% (w/v) GelMA precursor solution was placed in the barrel of a 1 mL syringe and light-cured at UV 405 nm for 6 s, respectively. To observe the microstructures of the GelMA constructs, the constructs were cultured in GM for 7 days. Then, the constructs were frozen at −20 °C for 24 h and subsequently −80 °C for 2 h. The frozen constructs were placed in a vacuum freeze dryer (SCIENTZ, China) for 24 h and then observed via scanning electron microscopy (SEM; HITACHI, Japan). The average pore size and total porosity of the hydrogels were measured using ImageJ software.

To determine the viability of DPSCs in different concentrations of GelMA constructs, DPSCs ($1×10^3$ cells/μL) were mixed with 6%, 9% or 12% (w/v) GelMA precursor solution. The cells/GelMA solution was injected into a 48-well plate (200 μL/well) with three wells for each group and cured by ultraviolet (UV) at 405 nm for 6 s to form cells/GelMA constructs, which were then incubated in GM. A CCK-8 assay was performed to evaluate the viability of DPSCs in GelMA scaffolds after 2, 5, and 8 days of incubation. The cells/GelMA constructs were incubated with CCK-8 working solution (600 μL/well) at 37 °C for 2 h, after which the reaction mixture was transferred to a 96-well plate (100 μL/well). Then, the absorbance at 450 nm was detected using a microreader (Tecan, Switzerland).

To evaluate whether cells in GelMA constructs have full access to the nutrition or medicine in the culture medium, DPSCs/Gel constructs in the GM group were cultured in GM, while the constructs in the other group were cultured with GM containing the 200 nM apoptosis-inducing drug staurosporine (STS; Sigma–Aldrich, USA) after three days of incubation in GM (GM+STS group), which served as an apoptosis positive control. Live/dead staining was then performed to evaluate the cell viability of the DPSCs/Gel constructs using the Calcein/PI Cell Viability Assay Kit (Beyotime, China) after 24 h. These constructs were observed and photographed using an inverted fluorescence microscope (Nikon, Japan).

To examine the differentiation capacity of DPSCs in GelMA, we constructed DPSCs-loaded GelMA with or without GOQDs, and incubated them in OM with or without GOQDs. The medium was changed every 2 days, and ALP staining was carried out after 8 days.

Animal Experiment

Six-week-old male Spraque–Dawley rats (180 to 200 g weight; SPF Biotechnology Co., Ltd., Beijing, China) were used. The animal experiment was approved by the Institutional Animal Care and Use Committee of China Medical University (Issue No. CMU2021351). All in vivo experimental procedures in this study were performed in accordance with the US Public Health Service Policy on Humane Care and Use of Laboratory Animals. The rats were randomly divided into 5 groups according to the implants, with six rats in each group. Model group: no material; Gel group: GelMA immersed in OM for 8 days; GOQDs/Gel group: GelMA containing GOQDs immersed in GOQDs-contained OM for 8 days; DPSCs/ Gel group: GelMA loaded with DPSCs cultured in OM for 8 days; GOQDs/DPSCs/Gel group: GOQDs-contained GelMA loaded with DPSCs cultured in GOQDs-contained OM for 8 days. All the implants were fabricated as cylinders with a diameter of 5 mm and a height of 1 mm. Approximately 20 μL of hydrogel is required to prepare such a piece of cylinder. The concentration of cells within the hydrogel was $1×10^3$ cells/μL. Accordingly, $2×10^4$ DPSCs were implanted in each rat's bone defect in the DPSCs/Gel and GOQDs/DPSCs/GelMA groups. The concentration of GelMA was 6% and that of GOQDs within GelMA construct is 5 μg/mL. Accordingly, the dose of GelMA implanted in each rat was 1.2 mg; the dose of GOQDs was 0.1 μg per rat in the GOQDs/Gel group and GOQDs/DPSCs/Gel group. An inhalation anesthesia machine (RWD, China) was loaded with isoflurane (RWD, China) to anesthetize the rats. The area of the cranial vault from the line connecting the outer corners of the eyes to the line connecting the two ear holes was shaved, and the skin was disinfected alternately with 75% alcohol. The skin, subcutis, and periosteum were incised along the sagittal midline of the cranial vault to expose the cranial vault bone, and the calvarial bone defect was modeled with an

osteotomy drill with an outer diameter of 5 mm on the left side of the sagittal suture. During surgery, saline drops were continuously applied to the operative area to cool it down and prevent thermal damage to the bone tissue and brain. Damage to the dura mater and sagittal sinus was avoided during the operation. Implantation was performed according to grouping. The wound was closed in layers via 6–0 absorbable sutures. Rats were sacrificed three weeks after surgery via inhalation of excess carbon dioxide, and the calvarial bone was removed and fixed with 4% paraformaldehyde at room temperature for 24 h. Micro-computed tomography (CT) scanning was performed, followed by decalcification, embedding and sectioning.

Micro-CT Analysis

Micro-CT was used to scan the calvarial bone of the rats according to an imaging rotation of 360° with an operating voltage of 70 kV and an operating current of 200 μA, and images were obtained. The images were adjusted to a suitable angle using DataViewer software, the tomographic images were analyzed, the newborn bone volume was calculated using CtAn software, and the tomographic images were reconstructed into three-dimensional images using CtVox software. The volume and surface density of new bone were subsequently statistically analyzed.

Histological Analysis

For hematoxylin and eosin (HE) staining, the deparaffinized and hydrated sections were stained with hematoxylin (Servicebio, China) for 5 min, and rinsed in tap water for 3 min. The sections were soaked in 75%, 85% and 95% (v/v) ethanol for 2 min, respectively. Then, the sections were stained with eosin (Servicebio, China) for 10 min, dehydrated twice in ethanol for two times and finally sealed with neutral gum. Masson's trichrome staining was performed according to instructions of the Masson's Trichrome Staining Kit (Baso, China). Immunohistochemical staining was performed according to the instructions of the DAB detection kit (Genetech, China). The deparaffinized and hydrated sections were incubated in pepsin (MXB, China) at 37 °C for 30 min for antigen repair and stained with osteocalcin (OCN) antibody (Affinity, China) at 4 °C overnight for further evaluation.

Transmission Electron Microscopy (TEM)

To determine whether treatment with GOQDs caused an increase in the number of mitophagosomes or mitolysosomes, DPSCs were cultured in OM with or without GOQDs for 24 h. Then, the cells were digested and centrifuged at 1000 rpm for 10 min. The cell pellets were fixed with 2.5% (w/v) glutaraldehyde (Servicebio, China) at 4 °C overnight, washed twice with 0.1 M sodium dimethylarsenate buffer for 10 min each time, fixed with 1% (w/v) osmium acid at 4 °C for 1.5 h, and washed twice with distilled water for 10 min each. The cell pellets were then dehydrated sequentially by alcohol at of 30%, 50%, 70%, and 90% (v/v) concentrations and acetone at 90% and 100% (v/v) concentrations (I, II, and III) for 10 to 15 min for each solution. Samples were sequentially permeated with 33%, 66%, and 100% (w/v) Epon812 resin (SPI, USA) diluted with acetone for 3 h at each concentration. The resin-impregnated samples were then cured in an oven at 37 °C for 12 h, 45 °C for 12 h, and 60 °C for 48 h. The samples were cut into 70-nm-thick sections using an ultrathin slicer (Leica, Germany). After staining was performed with lead citrate, the slices were examined and photographed using TEM (HITACHI, Japan).

Detection of Mitochondrial Membrane Potential (MMP)

JC-1 staining was performed to detect whether GOQDs treatment caused changes in MMP. JC-1 was a fluorescent probe indicative of MMP. When mitochondria are healthy, the MMP is high, and JC-1 aggregates in the mitochondrial matrix, in which it can form polymers and emit red fluorescence. However, when mitochondria are depolarized, the MMP is reduced, and JC-1 remains a monomer and emits green fluorescence. DPSCs were cultured in OM with or without GOQDs (5 μg/mL) or CsA (10 μM) for 24 h. The cells were then incubated in JC-1 working solution (30 μM; Bioquest, USA) at 37 °C for 30 min, washed with warm medium, and observed using an inverted fluorescence microscope. The ratio of red/green fluorescence was calculated using ImageJ software to evaluate the MMP.

Mitochondrial and Lysosomal Colocalization

To determine whether GOQDs treatment caused mitolysosomes to increase, DPSCs were cultured in OM or OM containing GOQDs (5 μg/mL) for 24 h, and the OM group was set as the control. To evaluate the effect of mitophagy inhibition on GOQDs-elicited osteogenesis, the cells were incubated in 5 μg/mL GOQDs-supplemented OM with or without cyclosporin A (CsA; 10 μM) for 24 h, with the group without CsA as the control. The cells were sequentially incubated with LysoTracker Red (75 nM; Beyotime, China), MitoTracker Green (200 nM; Beyotime, China) for 30 min, and Hoechst (Beyotime, China) for 10 min. The cells were then washed twice with prewarmed α-MEM in between, immersed in CM, and observed and photographed using an inverted fluorescence microscope (Nikon, Japan). The colocalization levels were indicated by Pearson's correlation coefficient (PCC) obtained from the semiquantitative analysis.

Statistical Methods

The details of the data analyses performed in this study are presented in the figure legends. Quantitative data are displayed as the mean ± standard deviation (represented as error bars) unless stated otherwise. A two-tailed Student's *t*-test was used to compare the differences between two groups. One-way analysis of variance (ANOVA) followed by Dunnett's post hoc test was used for comparisons among three or more groups. Differences were considered statistically significant when $P < 0.05$. For in vivo studies, rats were randomly assigned to treatment groups. All the experiments were conducted with at least three independent replicates unless stated otherwise.

Results

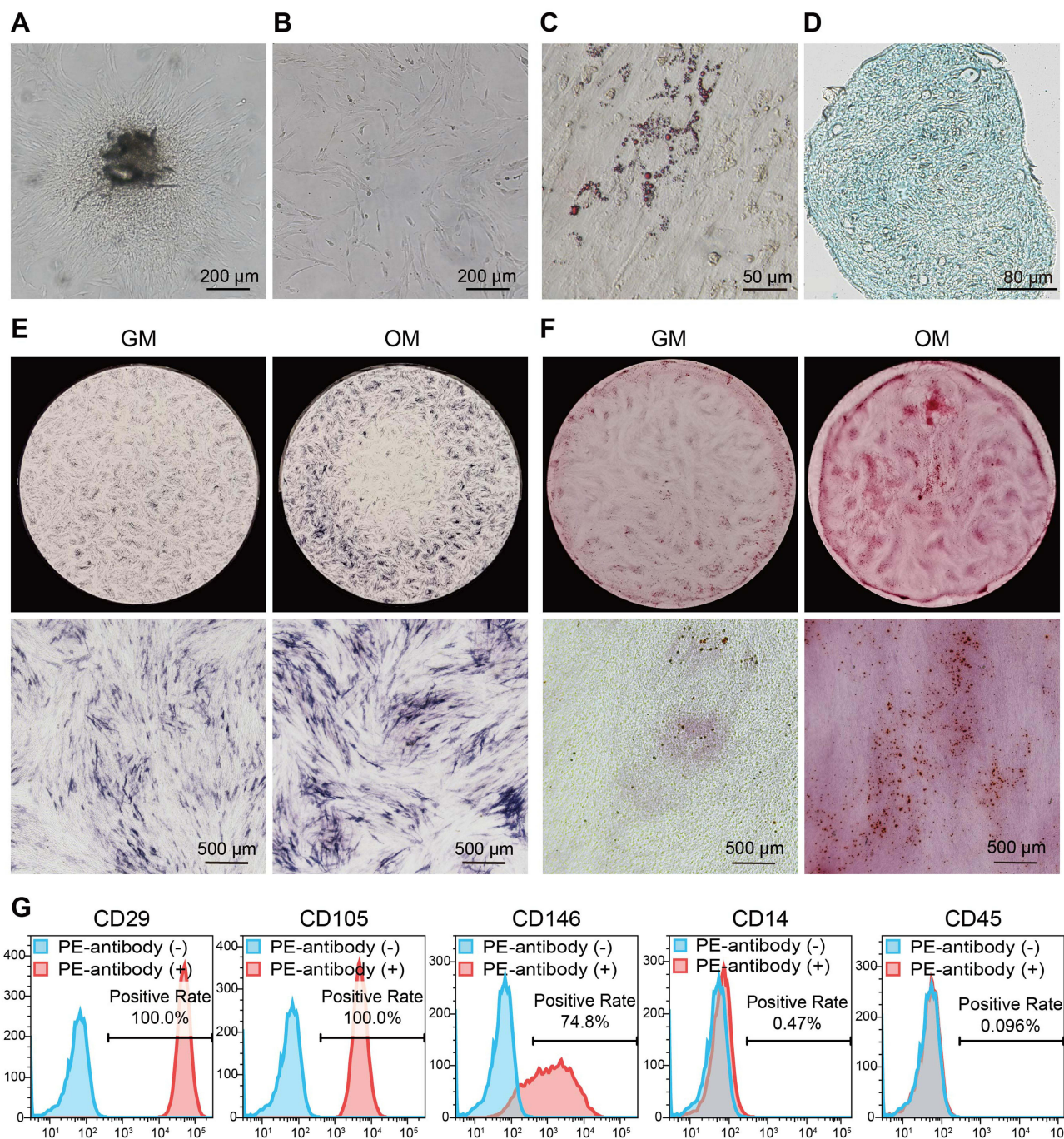## Isolation, Culture and Identification of DPSCs

We isolated and cultured dental pulp tissues and observed that many cells grew out of the tissues after 16 days (Figure 1A) and exhibited a fibroblast-like morphology (Figure 1B). The multipotency of these cells was subsequently assessed by inducing adipogenic, chondrogenic or osteogenic differentiation. Oil red O staining showed the formation of lipid droplets (stained red) in the cytoplasm, indicating that the cells differentiated into adipocytes (Figure 1C). Chondrogenic induction was also successful, as shown by Alcian blue staining of acidic mucopolysaccharide, which is secreted by chondroblasts (Figure 1D). ALP staining and ARS staining showed that ALP expression and the number of mineralized nodules in the OM-induced cells were greater than those in the GM group (Figure 1E and F), demonstrating that the cells underwent osteogenic differentiation. We next evaluated the mesenchymal origin of the cells through flow cytometry analysis, and the results showed that these cells positively expressed the MSCs surface marker molecules CD29 (100%), CD105 (100%), and CD146 (74.8%) but negatively expressed the hematopoietic markers CD14 (0.47%) and CD45 (0.096%) (Figure 1G). Based on the above data, the isolated and cultured cells were DPSCs, which are dental pulp-derived MSCs with multilineage differentiation potential.

Characterization of GOQDs

GOQDs are nearly spherical without sharp edges and are 4–18 nm in diameter as observed in the present study (Figure 2A and B). The AFM image (Figure 2C) and height profile (Figure 2D) revealed that the height of the delineated GOQDs was approximately 3.5 nm. The three-dimensional reconstructed image confirmed this analysis of the AFM images (Figure 2E). The PL properties of GOQDs are due to their nanoparticle size and surface status. For PL spectroscopy, excitation light in the wavelength range of 350–500 nm was used, and the results demonstrated that GOQDs are photoluminescent and emit different fluorescent signals when subjected to different wavelengths of excitation light (Figure 2F). Furthermore, GOQDs show the best emission when excited at 470 nm and emitted at 540nm. GOQDs solution emitted a weak yellow fluorescence when it was irradiated with 405-nm UV light (Supplementary Figure S1A), which verified the results of the PL spectroscopy.

GOQDs exhibit excellent dispersion in water without forming bulky aggregates that can damage cells (Figure S1B). The good dispersion of GOQDs may be related to the functional groups on their surface. The XPS full-spectrum scan results showed that the surface of GOQDs contained abundant oxygen (68.58%) (Figure 2G). The trace amounts of

Figure 1 Isolation, culture and identification of DPSCs. (**A**) A representative photo of primary colonies after 16 days (scale bar = 200 μm). (**B**) A representative photo of the first passage of DPSCs (scale bar = 200 μm). (**C**) A representative image of Oil Red O staining after adipogenic induction (scale bar = 50 μm). Lipid droplets were stained red. (**D**) A representative image of Alcian blue staining after chondrogenic induction (scale bar = 80 μm). Acidic mucopolysaccharides were colored blue. (**E**) Representative images of ALP staining after induction with osteogenic medium (OM group) or not (GM group) (scale bar = 500 μm). (**F**) Representative images of ARS staining (scale bar = 500 μm). The mineralized nodules were stained red. (**G**) Characterization of the DPSCs immunophenotype by flow cytometry.

calcium (Ca) and sodium (Na) were doped during the preparation process, while the neodymium (Nd) and silicon were contaminants caused by the XPS detection process. The fine spectrum scanning of O 1s (Figure 2H) revealed significant peaks at 531.1–531.8 eV (indicating C=O) and 532.3–533.3 eV (indicating C–O–H and C–O–C). The fine spectrum of C1s (Figure 2I) showed significant peaks at 284.6 eV (representing C–H and C–C), 286.1 eV (representing C–O–H and C–O–C), and 287.6 eV (representing C=O). Analysis of fine spectra data revealed that the surface of GOQDs contained
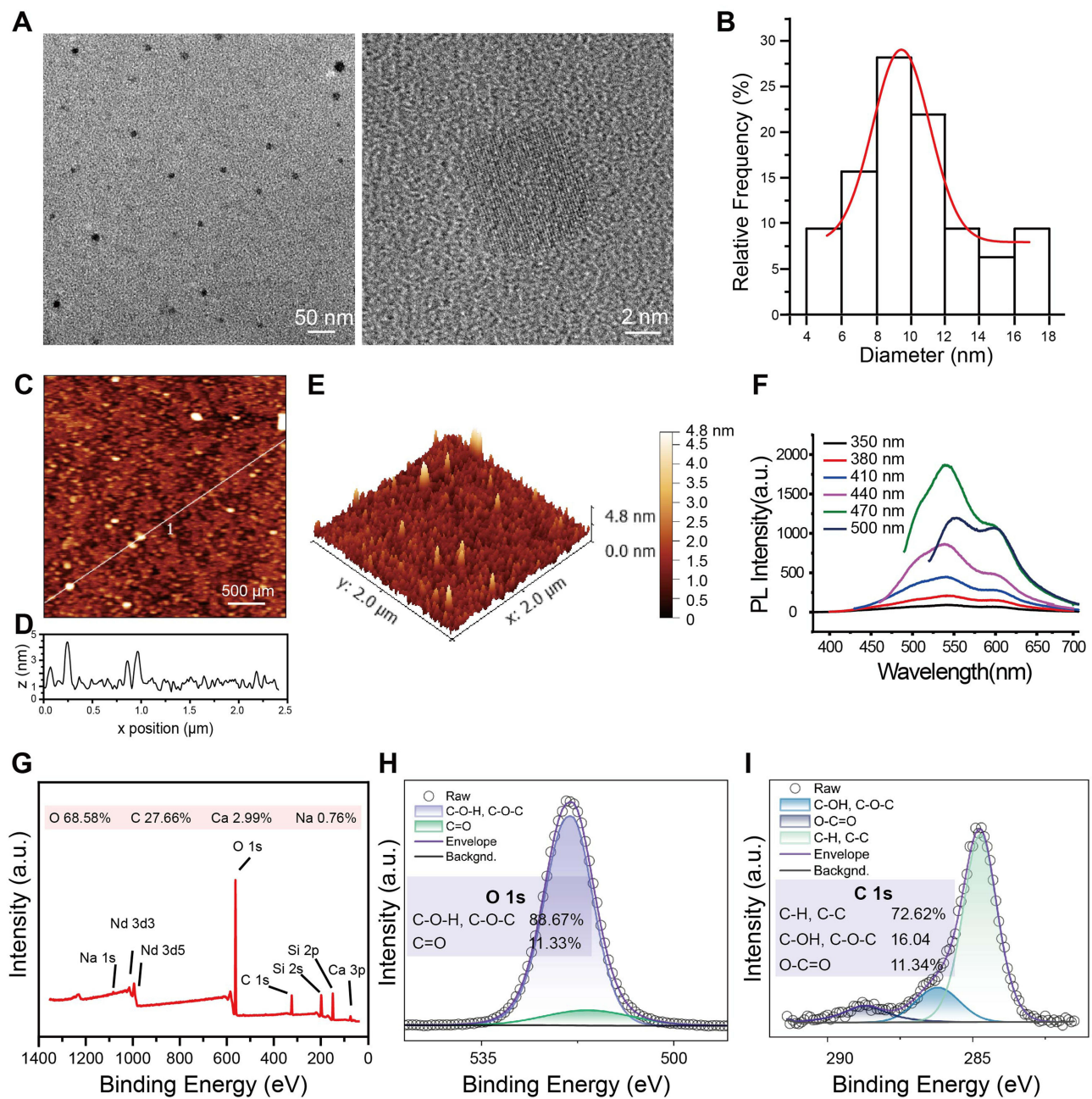
Figure 2 Characterization of GOQDs. (**A**) HRTEM image of the GOQDs dispersion (1 mg/mL) (scale bar of the left photo = 50 nm; scale bar of the right photo = 2 nm). (**B**) Histogram of the particle size distribution obtained by analyzing HRTEM images. (**C**) An AFM image showing the height of GOQDs (scale bar = 500 μm). (**D**)The height profile at the positions indicated by the white line. (**E**) Three-dimensional reconstructed AFM image of GOQDs. (**F**) PL spectrum of GOQDs. The lines in different colors indicate the different excitation light at various wavelengths, and the abscissa was the wavelength of the emitted light. (**G**) Full-spectrum XPS image of GOQDs. (**H**) Fine-spectrum XPS scans for oxygen (O 1s). (**I**) Fine-spectrum XPS scans for carbon (C 1s).

many oxygen-containing groups, mainly C–O–H and C–O–C, followed by O–C=O. The above results indicate that the surface of GOQDs contains abundant oxygen-containing groups, which may confer unique biological functions to GOQDs.

Effects of GOQDs on the Viability, Osteogenesis, and Migration of DPSCs

We performed a CCK-8 assay to detect the viability of DPSCs treated with various concentrations of GOQDs, and to determine the safe dose of GOQDs for DPSCs. Treating DPSCs with 0.5, 1, or 5 μg/mL GOQDs had no statistically

significant effect on their viability from 1 to 7 days, whereas significantly inhibited cell proliferation was detected in the 10 μg/mL group on days 1 and 7 and in the 20 μg/mL group on days 1, 4, and 7 (Figure 3A). Although the proliferation rate of the cells in the 10 and 20 μg/mL groups was lower than that in the control group, the cells were still proliferating and did not show obvious morphological damage on day 7, as shown in their photographs (Supplementary Figure S2). ALP staining and ALP activity assays after 8 days of induction showed that GOQDs at concentrations ranging from 5 to 20 μg/mL significantly promoted the ALP activity of DPSCs (Figure 3B and C). ARS staining and quantitative analysis of the mineralized nodules after 21 days of induction also confirmed that the same promotion trend of GOQDs (Figure 3D and E). The relative protein expression levels of Col-1 and OPN, which are late-stage biomarkers of osteogenic differentiation, were significantly enhanced by treatment with 1–20 μg/mL GOQDs (Figure 3F–H). Interestingly, our results revealed that although 10 and 20 μg/mL of GOQDs led to a significant slowdown of cell proliferation, they still significantly enhanced osteogenic differentiation. The inhibitory effect of these two concentrations of GOQDs on protein signaling associated with cell proliferation did not affect the activation of osteogenic differentiation signaling pathways. To determine the effect of GOQDs on the migration of DPSCs, we performed scratch experiments. The results indicated that 20 μg/mL GOQDs significantly impaired the migration ability of DPSCs, whereas 1 to 10 μg/mL GOQDs exhibited no significant effect on the migration of DPSCs (Figure 3I and J).

## In vitro Growth and Differentiation Capacity of DPSCs in GelMA

According to the above results, 5 μg/mL was confirmed to be the optimal concentration of GOQDs for promoting osteogenic differentiation in vitro, and we then examined the ability of GOQDs to promote bone repair in vivo. To determine the optimal concentration of GelMA for use as a scaffold, the pore sizes of different concentrations of the hydrogels were observed via SEM. The cross-sectional SEM images, average pore size analysis and porosity analysis showed that the 6% (w/v) GelMA group exhibited the largest pores and highest porosity among all of the tested groups (Figure 4A–C). The viability of DPSCs loaded with the three concentrations of GelMA was determined through the CCK-8 assay, and the results showed that cells in the 6% (w/v) hydrogel exhibited the greatest viability (Figure 4D). Therefore, 6% (w/v) GelMA was adopted as the scaffold in the present study.

To evaluate whether the cells in the GelMA constructs had full access to the nutrition and drugs in the culture medium, live and dead viability staining was performed, in which live cells were stained with Calcein AM and dead cells with PI. The results demonstrated that the cells in the GM group were elongated and spindle shaped and rarely died; however, many more red-stained dead cells were observed in the GM+STS group (Figure 4E), which served as a positive control. The results showed that the cells encapsulated in GelMA grew well in GM, whereas they were induced to undergo apoptosis in STS-containing medium, indicating that the concentration and the duration of light-curing of GelMA that we adopted can ensure that the DPSCs within hydrogel construct have full access to the nutrition and drugs in the culture medium.

Next, the cells/hydrogel complexes were divided into DPSCs/Gel and GOQDs/DPSCs/Gel groups according to whether the culture medium and hydrogel contained GOQDs (5 μg/mL). This was performed to test whether DPSCs cultured in three dimensions within the hydrogel had the same osteogenic differentiation ability as DPSCs cultured on the two-dimensional plastic substrate. Staining images showed that the expression of ALP in the GOQDs/DPSCs/Gel group was much greater than that in the DPSCs/Gel group; ie, the addition of GOQDs to the culture medium and hydrogel promoted the differentiation of DPSCs, which corresponded with the results obtained from cells cultured in two dimensions (Figure 4F). These results indicate that we successfully constructed hydrogel scaffolds loaded with GOQDs and DPSCs and verified that GOQDs promoted the osteogenic differentiation of DPSCs under three-dimensional culture conditions.

GOQDs/DPSCs/Gel Promoted Bone Regeneration in vivo

To evaluate the effects of GOQDs on bone regeneration in vivo, nothing (Model), GelMA (Gel), GOQDs-laden GelMA (GOQDs/Gel), DPSCs-laden GelMA (DPSCs/Gel), or GOQDs- and DPSCs-laden GelMA (GOQDs/DPSCs/Gel) were implanted into the calvarial bone defects of the rats for 3 weeks (Figure 5A). To create the rat calvarial bone defect, we prepared a unilateral defect of 5–6 mm in diameter to avoid bleeding caused by damaging the sagittal suture
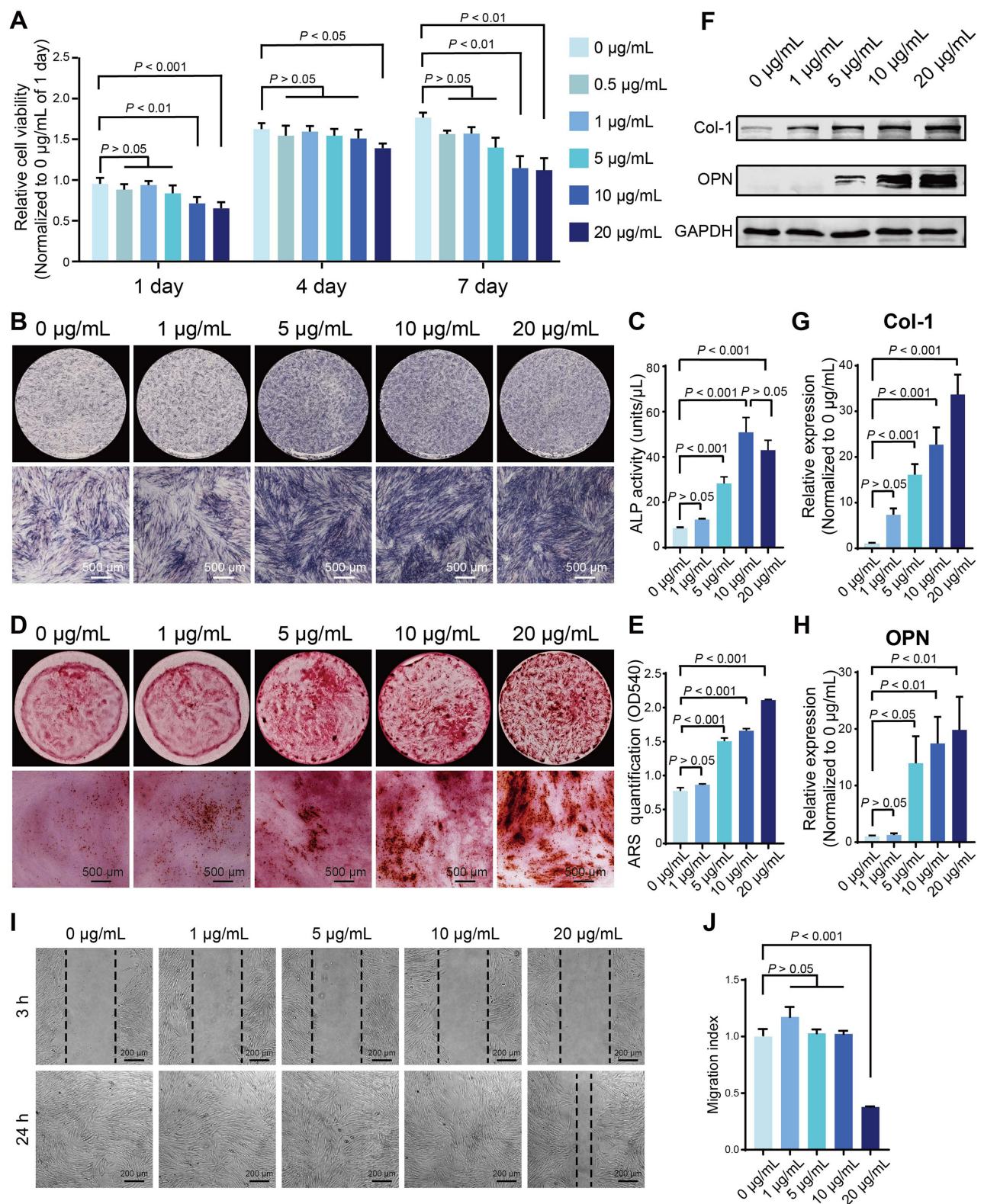
Figure 3 Effect of GOQDs on the viability, osteogenic differentiation, and migration of DPSCs in vitro. (**A**) CCK-8 analysis showing the effect of different concentrations of GOQDs on the viability of DPSCs (n = 3). (**B–H**) Effects of different concentrations of GOQDs on the osteogenic differentiation of DPSCs. (**B**) Representative ALP staining images (scale bar = 500 μm). (**C**) ALP activity assay (n = 3). (**D**) Representative ARS staining images (scale bar = 500 μm). (**E**) Quantitative analysis of mineralized nodules stained with ARS (n = 3) (**F**) Representative Western blot images showing the effect of GOQDs on osteogenic marker molecules in DPSCs. (**G**) The relative expression levels of Col-1 in (**F**) (n = 3). (**H**) The relative expression levels of OPN in (**F**) (n = 3). (**I**) Representative images of DPSCs at 3 h and 24 h after scratching (scale bar = 200 μm). (**J**) Migration indices of DPSCs treated with different concentrations of GOQDs (n = 3).

10117
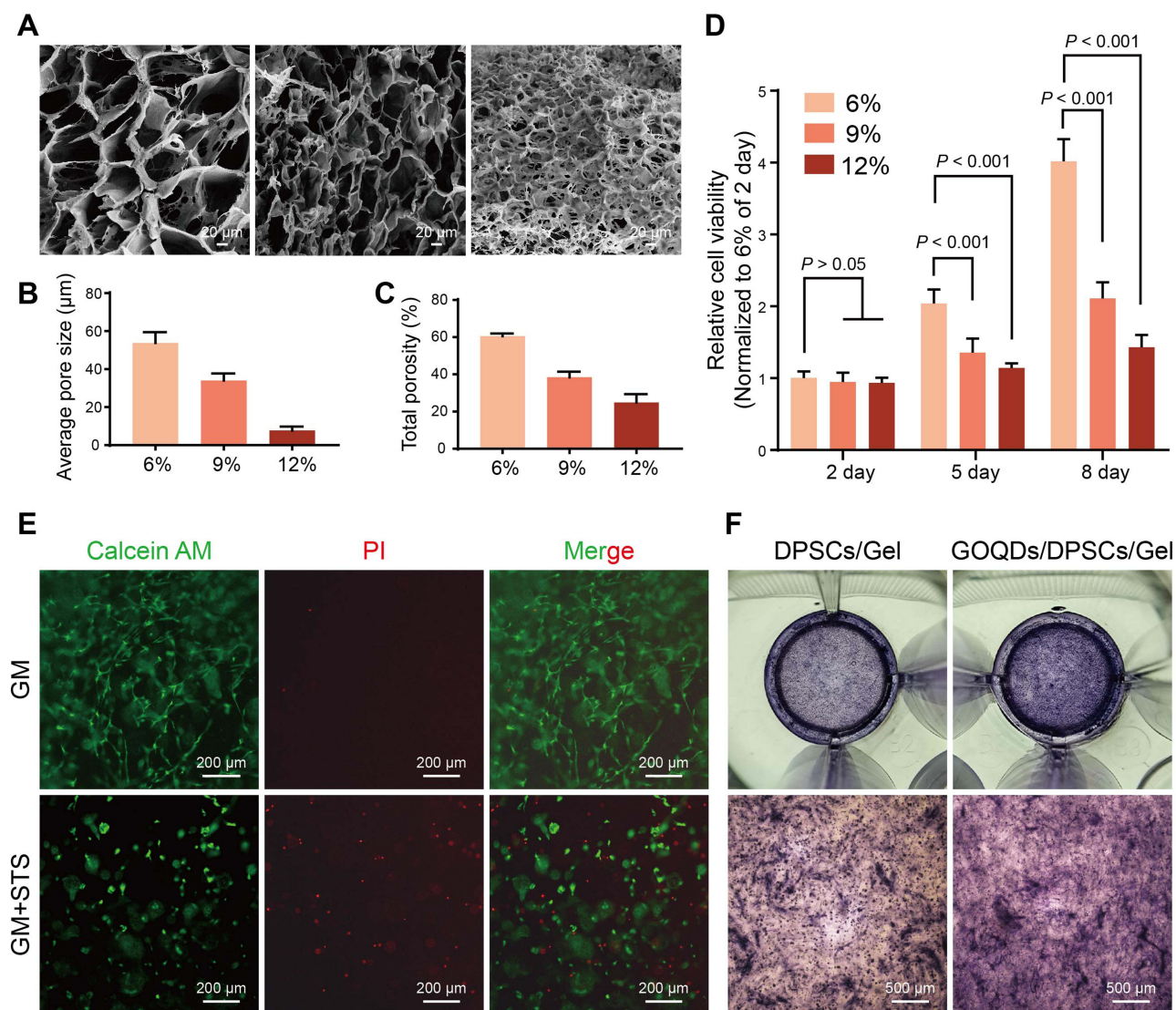
Figure 4 In vitro growth and differentiation capacity of DPSCs in GelMA. (**A**) Representative SEM images of different concentrations of GelMA (scale bar = 20 μm). (**B, C**) Average pore size and porosity of the hydrogels. (**D**) CCK-8 assay of DPSCs cultured in different concentrations of GelMA (n = 3). (**E**) Representative Calcein AM/PI fluorescence images of DPSCs/hydrogel complexes incubated with GM or GM containing 200 nM STS (GM+STS group) (scale bar = 200 μm). The GM+STS group served as a positive control to evaluate whether cells encapsulated in GelMA had full access to the drugs in the medium. The live cells were stained with Calcein AM (green), and the dead cells were stained with PI (red). (**F**) Representative ALP staining images of DPSCs/hydrogel complexes (scale bar = 500 μm). Neither the culture medium nor the hydrogel contained 5 μg/mL GOQDs in the DPSCs/Gel group, whereas both the culture medium and hydrogel contained 5 μg/mL GOQDs in the GOQDs/DPSCs/Gel group.

(Supplementary Figure S3). The effectiveness of bone repair was visualized and quantified via micro-CT. Limited bone regeneration was observed in the Model group, and newly formed bone was observed only at the edges of the defect. Nearly identical amounts of new bone were observed in the Gel, GOQDs/Gel, and DPSCs/Gel groups, and the amounts of these groups were greater than that of the Model group. In comparison, the greatest amount of newly formed bone among the five groups was detected in the GOQDs/DPSCs/Gel group, indicating that GOQDs-induced DPSCs exhibited powerful bone regeneration ability in vivo (Figure 5B–D). HE staining of the disembodied cranium confirmed that fibrous connective tissue had formed in the defects of the Model group. The largest volume of regenerated bone was observed in the GOQDs/DPSCs/Gel group, and many bone lacunae were clearly visible in the bone matrix (Figure 5E and F). As revealed by Masson's trichrome staining, the GOQDs/DPSCs/Gel group exhibited the greatest collagen deposition, suggesting that the greatest amount of immature bone tissue was present (Figure 5G and H). Additionally, the IHC staining results revealed that the defects in the GOQDs/DPSCs/Gel group exhibited the largest OCN-positive bone
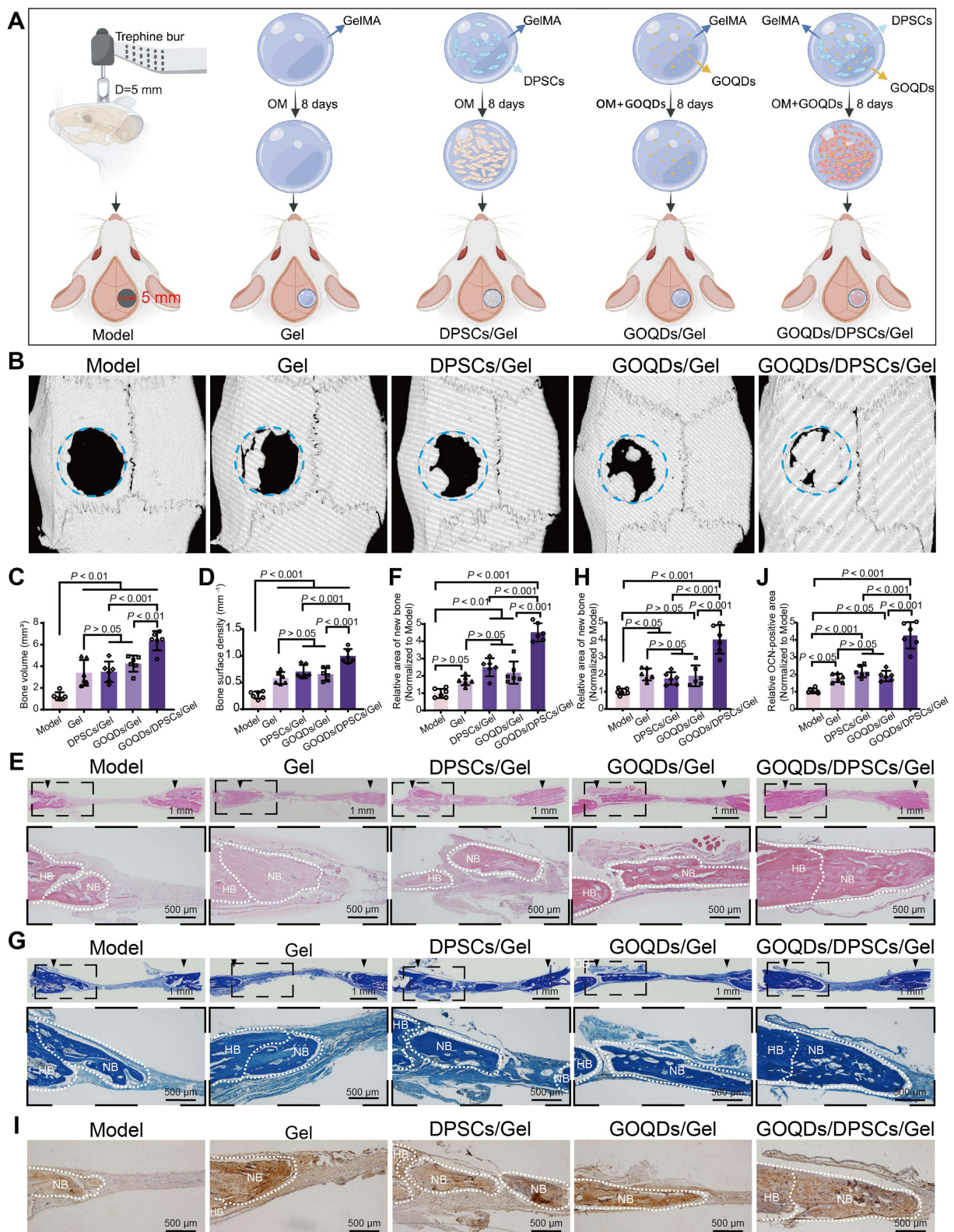
Figure 5 GOQDs/DPSCs/Gel promoted bone regeneration in vivo. (**A**) Grouping and flow of animal experiments (created with Biorender.com). (**B**) Three-dimensional reconstructed micro-CT images. (**C**) New bone volume at the defect site was calculated from micro-CT data (n = 6). (**D**) The surface density of new bone at the defect site was calculated from micro-CT data (n = 6). (**E**) Representative HE staining images (scale bar of the upper panel = 1 mm; scale bar of the lower panel = 500 μm). (**F**) The semiquantitative analysis of the new bone area in HE staining images (n = 6). (**G**) Representative Masson's trichrome staining images (scale bar of the upper panel = 1 mm; scale bar of the lower panel = 500 μm). (**H**) The semiquantitative analysis of the area of the newly formed immature collagen in Masson's trichrome staining images (n = 6). (**I**) Representative images of immunohistochemical staining for OCN (scale bar = 500 μm). (**J**) The semiquantitative analysis of the OCN-positive area in the immunohistochemical staining for OCN images (n = 6). NB indicates the newly formed bone (NB). HB indicates the host's bone (HB).

area (Figure 5I and J). These experimental results demonstrated that calvarial bone defects of 5 mm in diameter in rats cannot easily heal on their own within 3 weeks. However, the GOQDs/DPSCs/Gel construct accelerated the repair of the calvarial bone defects by inducing the greatest amount of newly generated bone. Compared to the transplantation of GOQDs/Gel constructs, which are acellular implants, the transplantation of GOQDs-preactivated DPSCs in GOQDs/DPSCs/Gel constructs repaired bone defects more efficiently.

GOQDs Promoted Mitophagy in DPSCs

The molecular mechanism by which GOQDs promote the osteogenic differentiation of DPSCs has yet to be elucidated. To further explore the biological mechanisms by which GOQDs promote the osteogenic differentiation of DPSCs, TEM images of DPSCs incubated with or without GOQDs were compared. We were surprised to discover that more mitochondria were engulfed by lysosomes (indicated by orange arrowheads) in GOQDs-incubated DPSCs (Figure 6A), which may imply that mitophagy in DPSCs has been influenced. JC-1 staining was performed to detect the changes in the MMP induced by GOQDs. Staining revealed that a decreased MMP occurred in the GOQDs-treated DPSCs (Figure 6B and C), which indicated that mitophagy was initiated. Consistent with the above observation, a significantly greater degree of colocalization of mitochondria and lysosomes was detected in DPSCs treated with GOQDs for 24 h, which was indicated by the overlap of yellow fluorescence (Figure 6D) and the PCC (Figure 6E). Accordingly, increased expression levels of PINK1, PRKN, and p62 and an increased LC3 II/I ratio were detected in GOQDs group (Figure 6F–J). The above data suggested that the level of mitophagy increased upon GOQDs induction.

Mitophagy Inhibition Weakened the GOQDs-Induced Osteogenic Differentiation of DPSCs

To further demonstrate that mitophagy is a key regulatory target of GOQDs, we treated GOQDs-induced DPSCs with or without CsA. CsA inhibits the MMP transition, thereby hindering the early stage of mitophagy. The effectiveness of CsA in inhibiting mitophagy was first examined. JC-1 staining images demonstrated that CsA effectively inhibited the reduction in the MMP caused by GOQDs (Figure 7A and B). The fluorescence showed that CsA significantly inhibited the GOQDs-triggered colocalization of mitochondria and lysosomes (Figure 7C and D), and this change was accompanied by a decrease in the expression of mitophagy hallmarks (Figure 7E–I). Therefore, 10 μM CsA effectively inhibited GOQDs-induced mitophagy. The effect of CsA-mediated mitophagy inhibition on GOQDs-induced osteogenesis was then determined by Western blotting and ALP staining. The results showed that CsA markedly attenuated the expression of the osteogenic marker proteins Runx2 and Osx (Figure 7J–L) and the GOQDs-induced increase in ALP activity (Figure 7M). These results indicated that mitophagy inhibition weakened the GOQDs-induced osteogenic differentiation of DPSCs.

Discussion

The acellular biological scaffolds may have limited efficacy in promoting bone regeneration, particularly when the intrinsic regenerative potential of the host's cells is compromised due to factors such as age and health.[21] Therefore, utilizing exogenous cells for bone repair remains a promising therapeutic strategy. MSCs have garnered great interest in cell therapy due to their multipotency, which is central to their therapeutic functions. MSCs derived from different tissue sources exhibit distinct characteristics.[22] DPSCs, which are derived from dental pulp tissue, benefit from the protective environment of the pulp cavity, allowing for the isolation of primary DPSCs while minimizing the risk of tissue contamination. This advantage provides DPSCs with a notable edge over other dental-derived stem cells, such as periodontal ligament stem cells and dental follicle progenitor cells. In addition, DPSCs are more readily accessible and exhibit greater clonogenic and proliferative potential compared to BMSCs.[2] Therefore, in this study, DPSCs were selected as the seed cells for the bone repair.

Bioactive factors are drugs that enhance the differentiation of seeded stem cells in BTE. GO exhibits osteogenic activity, a large surface area and excellent mechanical properties, with a single-layer Young's modulus exceeding 200 GPa.[23] Thus, the potential application of GO in BTE has attracted considerable attention.[24,25] However, GO is a two-
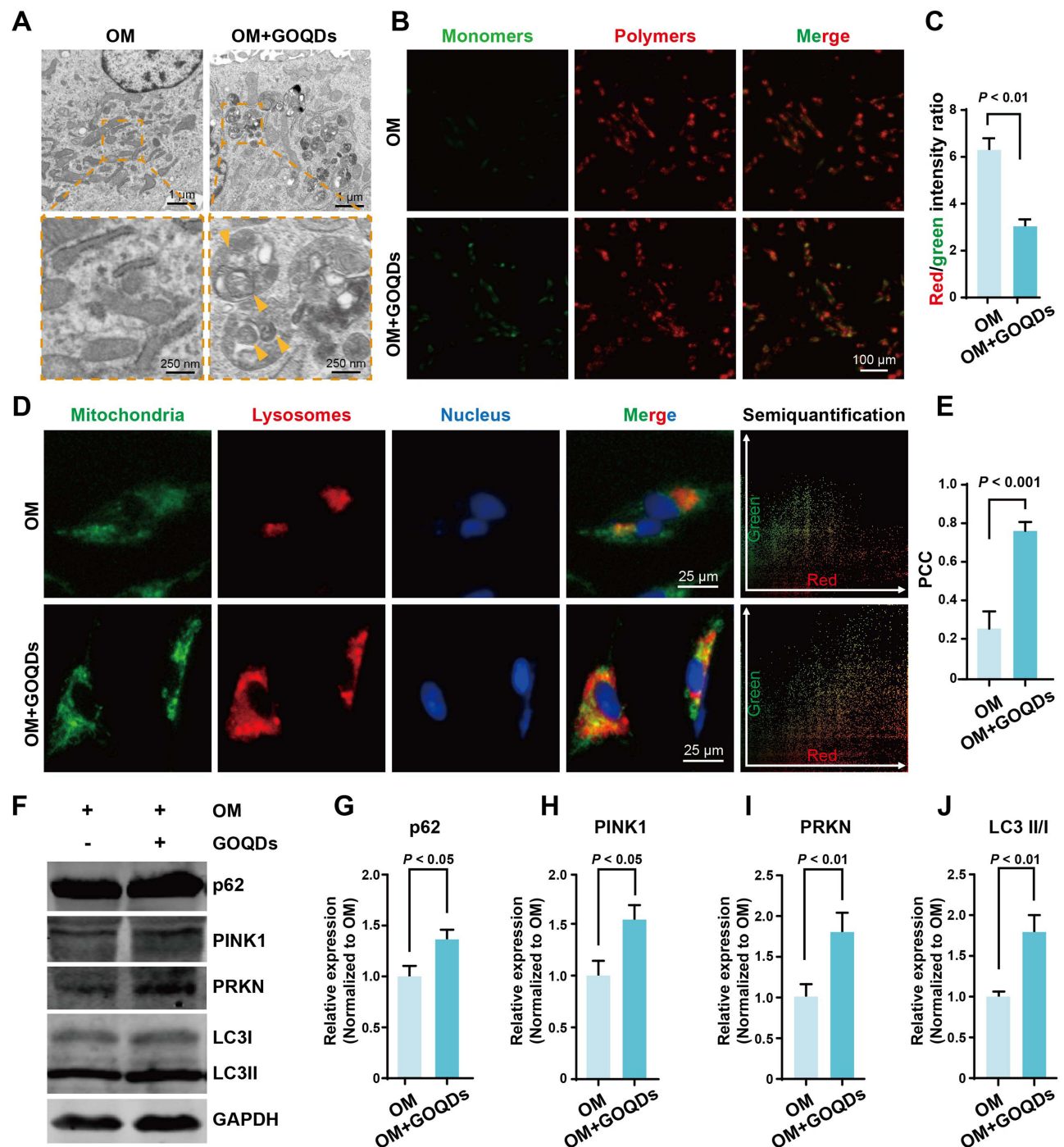
Figure 6 GOQDs promoted mitophagy in DPSCs. (**A**) Representative TEM images of DPSCs induced with or without GOQDs (scale bar of the upper panel = 1 μm; scale bar of the lower panel = 250 nm). The Orange arrowheads indicate the mitochondria engulfed by lysosomes. (**B**) Representative JC-1 staining images showing the influence of GOQDs on the MMP of DPSCs (scale bar = 100 μm). (**C**) Ratios of red/green fluorescence intensity were calculated to determine the MMP (n = 3). (**D**) Colocalization of mitochondria (green) and lysosomes (red) in DPSCs treated with or without GOQDs (scale bar = 25 μm). The colocalization scatterplot was obtained by analyzing the merge image using the Color2 plugin of ImageJ software. (**E**) Semiquantitative analysis of colocalization images (n = 3). (**F**) Representative Western blot images showing the effect of GOQDs induction on the expression of the mitophagy markers. (**G**) The relative expression levels of p62 in (**F**) (n = 3). (**H**) The relative expression levels of PINK1 in (**F**) (n = 3). (**I**) The relative expression levels of PRKN in (**F**) (n = 3). (**J**) The ratios of LC3II/I expression levels in (**F**) (n = 3).

dimensional nanosheet with lateral dimensions of 200–300 nm and sharp edges, which often causes mechanical damage to cells.[8] GOQDs are derivatives of GO that are reduced to the quantum scale. GOQDs synthesized using different methods can display significant variations in their particle size, surface functional groups, and photoluminescence
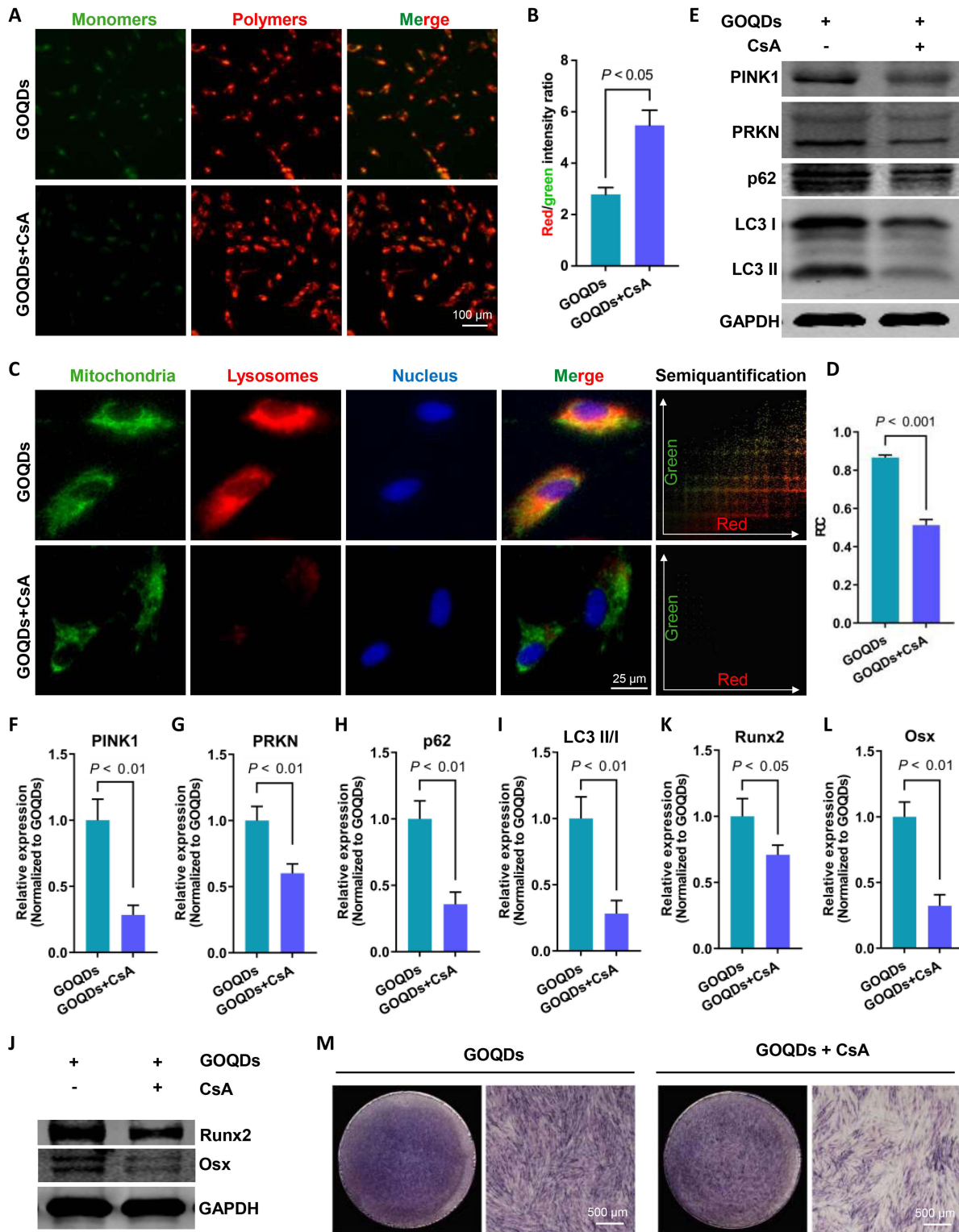
Figure 7 Mitophagy inhibition weakened GOQDs-induced osteogenic differentiation in DPSCs. (**A**) Representative JC-1 staining images showing the effect of CsA on the MMP of DPSCs (scale bar = 100 μm). (**B**) The semiquantitative analysis of JC-1 staining images (n = 3). The ratio of red/green fluorescence intensity indicates the MMP. (**C**) Representative fluorescence images showing the colocalization of mitochondria (green) and lysosomes (red) (scale bar = 25 μm) and the colocalization scatterplot, which was obtained by analyzing the merge image using the Color2 plugin of ImageJ software. (**D**) The semiquantitative analysis of the fluorescence colocalization images (n = 3). (**E**) Representative Western blot images showing the effect of CsA on the expression of mitophagy markers. (**F**) The relative expression levels of PINK1 in (**E**) (n = 3). (**G**) The relative expression levels of PRKN in (**E**) (n = 3). (**H**) The relative expression levels of p62 in (**E**) (n = 3). (**I**) The ratios of LC3 II/I expression levels in (**E**) (n = 3). (**J**) Representative Western blot images showing the effect of mitophagy inhibition on the expression of osteogenic transcription factors (n = 3). (**K**) The relative expression levels of Runx2 in (**J**) (n = 3). (**L**) The relative expression levels of Osx in (**J**) (n = 3). (**M**) Representative ALP staining images showing the effect of mitophagic inhibition on the ALP expression in DPSCs (scale bar = 500 μm).

characteristics.[26] The GOQDs used in this study were prepared using the modified Hummer's method, which involves the exfoliation of large graphite materials into nanosized quantum dots.[13,27] Our GOQDs are 4–18 nm in diameter and contain abundant oxygen-containing functional groups, including carboxyl and hydroxyl groups, which facilitate interactions with water molecules through hydrogen bonding.[28] This good dispersibility allows GOQDs to interact more efficiently with cells. In contrast to GO, the zero-dimensional size of GOQDs contributes to their excellent biocompatibility. Previous research has shown that GOQDs at concentrations below 200 μg/mL did not impair cell viability and were either degraded or excreted within 14 days without causing significant organ damage.[8,9] However, the noncytotoxic concentration determined in the present work (5 μg/mL) is lower than that reported in the literature mentioned above; these discrepancies may arise from variations in cell types and treatment durations. Approximately one week is typically required for the in vitro osteogenic differentiation of stem cells, making it particularly relevant to assess the biosafety of GOQDs when in contact with DPSCs over this duration. Additionally, the C−O groups of GOQDs (C−O−H/C−O−C) increase the number of reactive sites, especially hydroxyl groups. These strong electron donor groups are believed to accelerate the electron transfer process to H_2O_2 by reinforcing the delocalized electron density of the conjugated π system,[29,30] which might contribute to the production of intracellular ROS. Consequently, high concentrations of GOQDs may lead to a burst of intracellular ROS and inhibition of cell viability.

In this study, we found that 5 μg/mL of GOQDs significantly promoted differentiation without comprising cell viability. However, another study indicated that a minimum concentration of 10 μg/mL of GOQDs was necessary to promote osteogenic differentiation in DPSCs,[13] which contradicts our findings. This discrepancy may be attributed to the different methods of GOQDs production; the previous study utilized pyrolysis of citric acid, a bottom-up approach, while the GOQDs used in the present study were prepared using the modified Hummer's method, a top-down method. These two methods result in distinct particle sizes and functional groups, which account for the variations in effective concentrations.[31] The mechanism by which GOQDs promote osteogenic differentiation may involve the adsorption of proteins from biological environment (eg, culture media) onto the oxygen-containing functional groups on the nanomaterial surface, forming a protein corona.[32,33] The protein profile of the corona is determined by the charge, size and functional groups on the surface of the nanoparticles.[34,35] The biological effects of nanomaterials are strongly influenced by the nature of protein corona.[36] A previous study showed that proteins adsorbed onto the surface of GO in culture media were primarily associated with metabolic processes and signal transduction.[37] The C−O−C and C−O−H groups on the surface of GOQDs can interact with dexamethasone and ascorbic acid, both of which are critical agents for the osteogenesis of MSCs.[38–40] Dexamethasone synergizes with β-glycerolphosphate to activate the expression of ALP and other osteogenic proteins, while ascorbic acid acts as a cofactor for the synthesis of Col-1, facilitating biomineralization.[41] Therefore, the enrichment of dexamethasone and ascorbic acid by GOQDs effectively promotes osteogenic differentiation and biomineralization. Evaluating the effectiveness of bioactive factors involves not only their effect on stem cell differentiation but also their impact on cellular migration. The present work revealed that 1 to 10 μg/mL GOQDs exhibited no significant effect on the migration of DPSCs. This finding aligns with a previous study that similarly reported no significant effect of GOQDs on the migration ability of fibroblasts.[42] This result suggests that GOQDs may lack the ability to enhance cell migration, potentially limiting their therapeutic efficacy when used in isolation in vivo. Thus, combining GOQDs with exogenous stem cells may provide improved therapeutic outcomes compared to regimens that without exogenous seed cells.

Bioactive factors and seed cells need to be loaded into scaffolds before implantation at the defect site. As an analog of the extracellular matrix, the scaffold should possess a three-dimensional porous structure to facilitate nutrient delivery and promote cell growth.[43] Studies have shown that macroporous scaffolds not only provide extensive surface area for cell attachment but also support cell differentiation.[44] Hydrogel-based adhesives have been employed for sealing tissues or coating implants, enhancing their adhesion to surrounding tissues and increasing the invasion and retention of functional cells.[45] Therefore, we chose a highly porous GelMA hydrogel with macropores as a scaffold to ensure that DPSCs have full access to nutrients in the culture medium. Our experiments demonstrated that GOQDs can promote the osteogenic differentiation of DPSCs encapsulated in three-dimensions GelMA scaffold with a pore size of approximately 50 μm, confirming the successful construction of the GOQDs/DPSCs/Gel composite scaffold. Craniofacial bones primarily form through intramembranous ossification, wherein MSCs differentiate directly into osteoblasts and

subsequently develop into cancellous bone structures cross-linked by organic/inorganic hybridization.[46] We created a unilateral 5 mm round bone defect in the rat calvaria, which exhibited minimal self-healing over a three-week period. GOQDs-preactivated DPSCs within the GOQDs/DPSCs/Gel constructs demonstrated the most efficient repair of the bone defects. This finding supports our hypothesis that the combination of GOQDs with exogenous seed cells may mitigate the limitations of GOQDs in promoting cell migration and fully exploit their osteogenesis-promoting effect. Moreover, in this study, the GOQDs-treated DPSCs were cultured in vitro for 8 days prior to implantation. This incubation allows the DPSCs to differentiate into osteoblasts in a mild and stable environment, enabling them to secrete bone matrix more rapidly upon implantation and reducing potential hindrance to osteogenic differentiation that DPSCs may encounter in the harsh microenvironment of bone defects.[47] To our knowledge, this study is the first to validate the calvarial bone regeneration effect of GOQDs-activated exogenous stem cells in vivo. These results strongly indicate that GOQDs-preactivated DPSCs/Gel can effectively repair bone defects, providing a novel approach for the application of GOQDs in BTE.

Understanding the mechanism by which GOQDs promote the osteogenic differentiation of DPSCs is crucial for the targeted application of GOQDs in BTE. TEM revealed an increased probability of round, damaged mitochondria being encapsulated in lysosomes in GOQDs-activated DPSCs, implying that mitophagy was promoted. Mitophagy is a process that allows cells to eliminate damaged mitochondria through finely regulated signals and plays a critical role in mitochondrial quality control.[48] PINK1 and PRKN are key proteins involved in the ubiquitin-dependent mitophagy pathway.[48] When the MMP decreases, the PINK1 precursor is retained in the outer mitochondrial membrane and undergoes autophosphorylation, which recruits PRKN from the cytoplasm to the outer mitochondrial membrane and activates its E3 enzyme activity.[48] Subsequently, PRKN ubiquitinates outer mitochondrial membrane proteins, which are then phosphorylated by PINK1.[48] The phosphorylated, ubiquitin-modified outer membrane proteins are then recognized as "eat me" signals by autophagy receptors such as p62, NDP52, OPTN. These receptors bind to LC3 on the autophagosome membrane, bridging damaged mitochondria to the autophagosome and initiating mitophagy.[48–50] The present study demonstrated that mitophagy indicators, including PINK1, PRKN, p62, and LC3, are upregulated in GOQDs-preactivated DPSCs. This suggests that the activation of mitophagy may contribute to the enhanced osteogenic differentiation observed in these cells. Currently, no study has revealed how GOQDs promote mitophagy. Nonetheless, understanding the effect of GO on mitochondria may provide insight into the mechanism of GOQDs-induced mitophagy. GO exerts potent interlinking effects with the plasma membrane, allowing it to easily enter the cytoplasm and target at neuronal mitochondria, thereby inducing mitophagy.[51,52] The intracellular behavior of GOQDs may differ from that of GO, as GOQDs are quantum-dot in size with excellent dispersibility. This property makes them more prone to escape from lysosomes into the cytoplasm and then interact with mitochondria.[19,20] Therefore, GOQDs may have more opportunities to adhere to mitochondria and trigger elevated levels of mitophagy. The mechanism by which mitophagy promotes osteogenic differentiation may involve providing energy and metabolic support for osteogenesis. During osteogenic differentiation, the primary source for cellular energy transits from glycolysis to the mitochondrial oxidative phosphorylation (OXPHOS) pathway.[53,54] However, excessive OXPHOS produces high levels of reactive oxygen species (ROS), which can be detrimental to both mitochondria and cells, thereby hindering the continued differentiation of MSCs.[53–55] Mitophagy plays a crucial role in removing excessive ROS and clearing damaged mitochondria, facilitating the continuation of the differentiation process.[56,57] Our study demonstrated that the osteogenic differentiation of DPSCs was promoted following an increase in mitophagy levels, which is consistent with findings from previous research. Our experiments, alongside earlier studies, indicate that enhanced mitophagy significantly promotes the osteogenic differentiation of MC3T3 cells or DPSCs.[58,59] These findings suggest that not all damaged mitochondria are removed during osteogenic differentiation, and that enhanced mitophagy can further eliminate the residual damaged mitochondria. Therefore, mitophagy represents a promising target for regulating stem cell differentiation. Additionally, mitophagy fosters the renewal and remodeling of mitochondria by removing dysfunctional organelles, which contributes to conducive to the establishment of an efficient OXPHOS system and provides a stable energy source for cell differentiation. Furthermore, mitophagy plays an important role in mineralization stage by transporting amorphous calcium phosphate precursors from mitochondria to the extracellular matrix.[58] In summary, the present study innovatively proposed a mechanism underlying GOQDs-induced mitophagy-driven osteogenic differentiation of DPSCs.
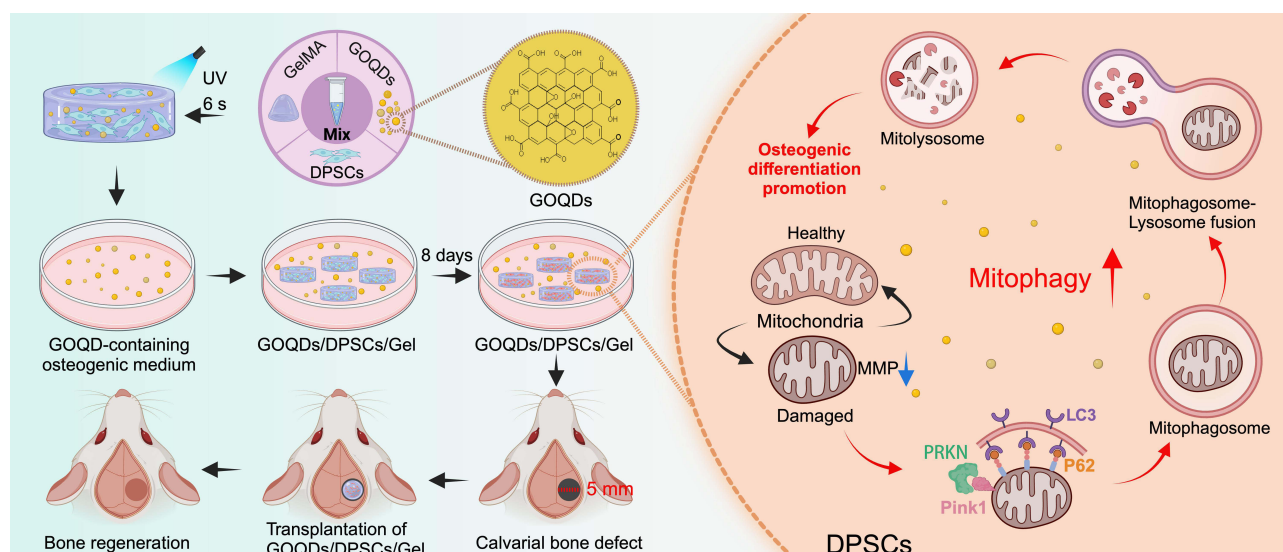
Scheme 1 Summary of DPSCs activated by GOQDs repair rat calvarial bone defect via promoting mitophagy-related osteogenic differentiation. GOQDs/DPSCs/GelMA hydrogel composites are incubated in GOQDs-containing medium in vitro for eight days and then implanted into calvarial bone defects. The GOQDs/DPSCs/GelMA composites effectively repair the bone defects. The underlying mechanism is revealed that GOQDs induce mitophagy in DPSCs, as evidenced by a decrease in MMP, up-regulation of the expression of PRKN, PINK1, LC3, and P62, and an increase in the co-localization of mitochondria and lysosomes. Then, the mitophagy-regulated osteogenic differentiation of DPSCs is promoted by GOQDs (created with Biorender.com).

Furthermore, it suggests that GOQDs could serve as agonists targeting stem cell mitophagy, presenting promising application in the surface modification and performance optimization of biomaterials for bone repair.

Conclusion

In summary, this study showed that GOQDs enhance the osteogenic differentiation of DPSCs and that the BTE substitute composed of GOQDs-preactivated DPSCs and GelMA accelerated bone regeneration in vivo. Importantly, we identified that the mechanism underlying GOQDs-induced osteogenesis is linked to improved PINK1/PRKN-mediated mitophagy flux, which is an uncharted signaling pathway in DPSCs exposed to GOQDs (Scheme 1). Collectively, our findings provide an operative approach for bone defect repair utilizing GOQDs as bioactive factors while uncovering the mechanism of GOQDs-elicited osteogenesis. Compared to traditional growth factors, GOQDs are cost-effective and simple to prepare, and their nanoscale size facilitates modification, making them well-suited for widespread application. In addition, by promoting mitophagy, GOQDs enhance stem cell osteogenic differentiation and therefore can be used as modulators of mitophagy in BTE, potentially offering a novel method for precise treatment of bone defects.

Abbreviations

AFM, atomic force microscopy; ALP, alkaline phosphatase; ANOVA, analysis of variance; ARS, alizarin red S; BMPs, bone morphogenetic proteins; BMSCs, bone marrow stem cells; BTE, bone tissue engineering; BV, bone volume; CM, complete medium; Col-1, collagen Type I; CsA, cyclosporin A; CT, computed tomography; DPSCs, dental pulp stem cells; FBS, fetal bovine serum; GelMA, gelatin methacryloyl; GOQDs, graphene oxide quantum dots; GO, graphene oxide; GM, growth medium; GAPDH, glyceraldehyde-3-phosphate dehydrogenase; HE, Hematoxylin & eosin; HRTEM, high-resolution field emission transmission electron microscope; IBMX, 3-isobutyl-1-methylxanthine; MMP, mitochondrial membrane potential; MSCs, mesenchymal stem cells; OM, osteogenic medium; OPN, osteopontin; OXPHOS, oxidative phosphorylation; PCC, Pearson's correlation coefficient; PE, phycoerythrin; PINK1, phosphatase-and-tensin homolog-induced putative kinase 1; PL, photoluminescence; PRKN, Parkin E3 ubiquitin ligase; SHEDs, stem cells from human exfoliated deciduous teeth; SEM, scanning electron microscopy; STS, staurosporine; TEM, transmission electron microscopy; TV, Tissue volume; UV, ultraviolet; WB, Western blot; XPS, X-ray photoelectron spectroscopy.

Data Sharing Statement

The datasets generated during and analyzed during the current study are not publicly available but are available from the corresponding author on reasonable request.

Funding

Disclosure

The authors report no conflicts of interest in this work.

References

1. Collins MN, Ren G, Young K, Pina S, Reis RL, Oliveira JM. Scaffold Fabrication Technologies and Structure/Function Properties in Bone Tissue Engineering. *Adv Funct Mater*. 2021;31(21):2010609. doi:10.1002/adfm.202010609
2. Gronthos S, Mankani M, Brahim J, Robey PG, Shi S. Postnatal human dental pulp stem cells (DPSCs) in vitro and in vivo. *Proc Natl Acad Sci U S A*. 2000;97(25):13625–13630. doi:10.1073/pnas.240309797
3. Leyendecker Junior A, Gomes Pinheiro CC, Lazzaretti Fernandes T, Franco Bueno D. The use of human dental pulp stem cells for in vivo bone tissue engineering: a systematic review. *J Tissue Eng*. 2018;9:2041731417752766. doi:10.1177/2041731417752766
4. Woo EJ. Adverse events after recombinant human BMP2 in nonspinal orthopaedic procedures. *Clin Orthop Relat Res*. 2013;471(5):1707–1711. doi:10.1007/s11999-012-2684-x
5. Visser R, Rico-Llanos GA, Pulkkinen H, Becerra J. Peptides for bone tissue engineering. *J Control Release*. 2016;244(Pt A):122–135. doi:10.1016/j.jconrel.2016.10.024
6. Safari B, Davaran S, Aghanejad A. Osteogenic potential of the growth factors and bioactive molecules in bone regeneration. *Int J Biol Macromol*. 2021;175:544–557. doi:10.1016/j.ijbiomac.2021.02.052
7. Tadyszak K, Musiał A, Ostrowski A, Wychowaniec JK. Unraveling origins of EPR spectrum in graphene oxide quantum dots. *Nanomaterials (Basel)*. 2020;10(4):798. doi:10.3390/nano10040798
8. Li J, Zhang X, Jiang J, et al. Systematic assessment of the toxicity and potential mechanism of graphene derivatives in vitro and in vivo. *Toxicol Sci*. 2019;167(1):269–281. doi:10.1093/toxsci/kfy235
9. He C, Jiang S, Yao H, et al. High-content analysis for mitophagy response to nanoparticles: a potential sensitive biomarker for nanosafety assessment. *Nanomedicine*. 2019;15(1):59–69. doi:10.1016/j.nano.2018.09.003
10. Daneshmandi L, Barajaa M, Tahmasbi Rad A, Sydlik SA, Laurencin CT. Graphene-based biomaterials for bone regenerative engineering: a comprehensive review of the field and considerations regarding biocompatibility and biodegradation. *Adv Healthc Mater*. 2021;10(1): e2001414. doi:10.1002/adhm.202001414
11. Alivisatos AP. Semiconductor clusters, nanocrystals, and quantum dots. *Science*. 1996;271(5251):933–937. doi:10.1126/science.271.5251.933
12. Xu D, Wang C, Wu J, et al. Effects of low-concentration graphene oxide quantum dots on improving the proliferation and differentiation ability of bone marrow mesenchymal stem cells through the Wnt/β-catenin signaling pathway. *ACS Omega*. 2022;7(16):13546–13556. doi:10.1021/acsomega.1c06892
13. Li X, Liu H, Yu Y, Ma L, Liu C, Miao L. Graphene oxide quantum dots-induced mineralization via the reactive oxygen species-dependent autophagy pathway in dental pulp stem cells. *J Biomed Nanotechnol*. 2020;16(6):965–974. doi:10.1166/jbn.2020.2934
14. Yang X, Zhao Q, Chen Y, et al. Effects of graphene oxide and graphene oxide quantum dots on the osteogenic differentiation of stem cells from human exfoliated deciduous teeth. *Artif Cells Nanomed Biotechnol*. 2019;47(1):822–832. doi:10.1080/21691401.2019.1576706
15. Yang X, Zhao Q, Chen J, et al. Graphene oxide quantum dots promote osteogenic differentiation of stem cells from human exfoliated deciduous teeth via the Wnt/β-catenin signaling pathway. *Stem Cells Int*. 2021;2021:8876745. doi:10.1155/2021/8876745
16. Sun H, Xu J, Wang Y, et al. Bone microenvironment regulative hydrogels with ROS scavenging and prolonged oxygen-generating for enhancing bone repair. *Bioact Mater*. 2023;24:477–496. doi:10.1016/j.bioactmat.2022.12.021
17. Ren D, Zhang Y, Du B, Wang L, Gong M, Zhu W. An antibacterial, conductive nanocomposite hydrogel coupled with electrical stimulation for accelerated wound healing. *Int J Nanomed*. 2024;19:4495–4513. doi:10.2147/IJN.S460700
18. Mukkala AN, Jerkic M, Khan Z, Szaszi K, Kapus A, Rotstein O. Therapeutic effects of mesenchymal stromal cells require mitochondrial transfer and quality control. *Int J Mol Sci*. 2023;24(21):15788. doi:10.3390/ijms242115788
19. Zhang B, Wei P, Zhou Z, Wei T. Interactions of graphene with mammalian cells: molecular mechanisms and biomedical insights. *Adv Drug Deliv Rev*. 2016;105(Pt B):145–162. doi:10.1016/j.addr.2016.08.009
20. Feng X, Chen L, Guo W, et al. Graphene oxide induces p62/SQSTM-dependent apoptosis through the impairment of autophagic flux and lysosomal dysfunction in PC12 cells. *Acta Biomater*. 2018;81:278–292. doi:10.1016/j.actbio.2018.09.057
21. Ho-Shui-Ling A, Bolander J, Rustom LE, Johnson AW, Luyten FP, Picart C. Bone regeneration strategies: engineered scaffolds, bioactive molecules and stem cells current stage and future perspectives. *Biomaterials*. 2018;180:143–162. doi:10.1016/j.biomaterials.2018.07.017
22. Hoang DM, Pham PT, Bach TQ, et al. Stem cell-based therapy for human diseases. *Signal Transduct Target Ther*. 2022;7(1):272. doi:10.1038/s41392-022-01134-4
23. Xue H, Zhang Z, Lin Z, et al. Enhanced tissue regeneration through immunomodulation of angiogenesis and osteogenesis with a multifaceted nanohybrid modified bioactive scaffold. *Bioact Mater*. 2022;18:552–568. doi:10.1016/j.bioactmat.2022.05.023
24. Liu X, Li L, Gaihre B, et al. Scaffold-free spheroids with two-dimensional heteronano-layers (2DHNL) enabling stem cell and osteogenic factor codelivery for bone repair. *ACS Nano*. 2022;16(2):2741–2755. doi:10.1021/acsnano.1c09688

25. Newby SD, Masi T, Griffin CD, et al. Functionalized graphene nanoparticles induce human mesenchymal stem cells to express distinct extracellular matrix proteins mediating osteogenesis. *Int J Nanomed*. 2020;15:2501–2513. doi:10.2147/IJN.S245801

26. Yuan JM, Zhao R, Wu ZJ, Li W, Yang XG. Graphene oxide quantum dots exfoliated from carbon fibers by microwave irradiation: two photoluminescence centers and self-assembly behavior. *Small*. 2018;14(20):e1703714. doi:10.1002/smll.201703714

27. Ahirwar S, Mallick S, Bahadur D. Electrochemical method to prepare graphene quantum dots and graphene oxide quantum dots. *ACS Omega*. 2017;2(11):8343–8353. doi:10.1021/acsomega.7b01539

28. Mohammadrezaei D, Golzar H, Rezai Rad M, et al. In vitro effect of graphene structures as an osteoinductive factor in bone tissue engineering: a systematic review. *J Biomed Mater Res A*. 2018;106(8):2284–2343. doi:10.1002/jbm.a.36422

29. Chen Y, Su R, Xu F, et al. Oxygen-containing functional groups in Fe3O4@three-dimensional graphene nanocomposites for enhancing H2O2 production and orientation to 1O2 in electro-Fenton. *J Hazard Mater*. 2024;470:134162. doi:10.1016/j.jhazmat.2024.134162

30. Cui L, Zhao X, Xie H, Zhang Z. Overcoming the activity–stability trade-off in heterogeneous electro-Fenton catalysis: encapsulating carbon cloth-supported iron oxychloride within graphitic layers. *ACS Catal*. 2022;12(21):13334–13348. doi:10.1021/acscatal.2c03571

31. An N, Yan X, Qiu Q, et al. Human periodontal ligament stem cell sheets activated by graphene oxide quantum dots repair periodontal bone defects by promoting mitochondrial dynamics dependent osteogenic differentiation. *J Nanobiotechnol*. 2024;22(1):133. doi:10.1186/s12951-024-02422-7

32. Li H, Wang Y, Tang Q, et al. The protein Corona and its effects on nanoparticle-based drug delivery systems. *Acta Biomater*. 2021;129:57–72. doi:10.1016/j.actbio.2021.05.019

33. Kopac T. Protein Corona, understanding the nanoparticle-protein interactions and future perspectives: a critical review. *Int J Biol Macromol*. 2021;169:290–301. doi:10.1016/j.ijbiomac.2020.12.108

34. Rahimi S, Chen Y, Zareian M, Pandit S, Mijakovic I. Cellular and subcellular interactions of graphene-based materials with cancerous and non-cancerous cells. *Adv Drug Deliv Rev*. 2022;189:114467. doi:10.1016/j.addr.2022.114467

35. Ekal NS, Patil R, Ranjan N, Bahadur P, Tiwari S. Oxidation state of graphene oxide nanosheets drives their interaction with proteins: a case of bovine serum albumin. *Colloids Surf B Biointerfaces*. 2022;212:112367. doi:10.1016/j.colsurfb.2022.112367

36. da Costa Marques R, Hüppe N, Speth KR, et al. Proteomics reveals time-dependent protein Corona changes in the intracellular pathway. *Acta Biomater*. 2023;172:355–368. doi:10.1016/j.actbio.2023.10.010

37. Franqui LS, De Farias MA, Portugal RV, et al. Interaction of graphene oxide with cell culture medium: evaluating the fetal bovine serum protein Corona formation towards in vitro nanotoxicity assessment and nanobiointeractions. *Mater Sci Eng C Mater Biol Appl*. 2019;100:363–377. doi:10.1016/j.msec.2019.02.066

38. Ren N, Li J, Qiu J, et al. Growth and accelerated differentiation of mesenchymal stem cells on graphene-oxide-coated titanate with dexamethasone on surface of titanium implants. *Dent Mater*. 2017;33(5):525–535. doi:10.1016/j.dental.2017.03.001

39. Lee WC, Lim CH, Shi H, et al. Origin of enhanced stem cell growth and differentiation on graphene and graphene oxide. *ACS Nano*. 2011;5 (9):7334–7341. doi:10.1021/nn202190c

40. Yang JW, Hsieh KY, Kumar PV, et al. Enhanced osteogenic differentiation of stem cells on phase-engineered graphene oxide. *ACS Appl Mater Interfaces*. 2018;10(15):12497–12503. doi:10.1021/acsami.8b02225

41. Langenbach F, Handschel J. Effects of dexamethasone, ascorbic acid and β-glycerophosphate on the osteogenic differentiation of stem cells in vitro. *Stem Cell Res Ther*. 2013;4(5):117. doi:10.1186/scrt328

42. Hou T, Ma H, Gao X, Sun H, Wang L, An M. Study on long-term tracing of fibroblasts on three-dimensional tissue engineering scaffolds based on graphene quantum dots. *Int J Mol Sci*. 2022;23(19):11040. doi:10.3390/ijms231911040

43. Zhang K, Liu Y, Zhao Z, et al. Magnesium-doped nano-hydroxyapatite/polyvinyl alcohol/chitosan composite hydrogel: preparation and characterization. *Int J Nanomed*. 2024;19:651–671. doi:10.2147/IJN.S434060

44. Swanson WB, Omi M, Zhang Z, et al. Macropore design of tissue engineering scaffolds regulates mesenchymal stem cell differentiation fate. *Biomaterials*. 2021;272:120769. doi:10.1016/j.biomaterials.2021.120769

45. Lu G, Xu Y, Liu Q, et al. An instantly fixable and self-adaptive scaffold for skull regeneration by autologous stem cell recruitment and angiogenesis. *Nat Commun*. 2022;13(1):2499. doi:10.1038/s41467-022-30243-5

46. Chai Y, Maxson RE Jr. Recent advances in craniofacial morphogenesis. *Dev Dyn*. 2006;235(9):2353–2375. doi:10.1002/dvdy.20833

47. Salhotra A, Shah HN, Levi B, Longaker MT. Mechanisms of bone development and repair. *Nat Rev Mol Cell Biol*. 2020;21(11):696–711. doi:10.1038/s41580-020-00279-w

48. Han R, Liu Y, Li S, Li XJ, Yang W. PINK1-PRKN mediated mitophagy: differences between in vitro and in vivo models. *Autophagy*. 2023;19 (5):1396–1405. doi:10.1080/15548627.2022.2139080

49. Maity J, Deb M, Greene C, Das H. KLF2 regulates dental pulp-derived stem cell differentiation through the induction of mitophagy and altering mitochondrial metabolism. *Redox Biol*. 2020;36:101622. doi:10.1016/j.redox.2020.101622

50. Uoselis L, Nguyen TN, Lazarou M. Mitochondrial degradation: mitophagy and beyond. *Mol Cell*. 2023;83(19):3404–3420. doi:10.1016/j.molcel.2023.08.021

51. Kang Y, Yin S, Liu J, et al. Nano-graphene oxide depresses neurotransmission by blocking retrograde transport of mitochondria. *J Hazard Mater*. 2022;424(Pt D):127660. doi:10.1016/j.jhazmat.2021.127660

52. Kang Y, Liu J, Yin S, et al. Oxidation of reduced graphene oxide via cellular redox signaling modulates actin-mediated neurotransmission. *ACS Nano*. 2020;14(3):3059–3074. doi:10.1021/acsnano.9b08078

53. Ito K, Suda T. Metabolic requirements for the maintenance of self-renewing stem cells. *Nat Rev Mol Cell Biol*. 2014;15(4):243–256. doi:10.1038/nrm3772

54. Teslaa T, Teitell MA. Pluripotent stem cell energy metabolism: an update. *EMBO j*. 2015;34(2):138–153. doi:10.15252/embj.201490446

55. Lin S, Yin S, Shi J, et al. Orchestration of energy metabolism and osteogenesis by Mg2+ facilitates low-dose BMP-2-driven regeneration. *Bioact Mater*. 2022;18:116–127. doi:10.1016/j.bioactmat.2022.03.024

56. Maity J, Barthels D, Sarkar J, et al. Ferutinin induces osteoblast differentiation of DPSCs via induction of KLF2 and autophagy/mitophagy. *Cell Death Dis*. 2022;13(5):452. doi:10.1038/s41419-022-04903-9

57. Chen L, Shi X, Xie J, et al. Apelin-13 induces mitophagy in bone marrow mesenchymal stem cells to suppress intracellular oxidative stress and ameliorate osteoporosis by activation of AMPK signaling pathway. *Free Radic Biol Med*. 2021;163:356–368. doi:10.1016/j.freeradbiomed.2020.12.235

58. Pei DD, Sun JL, Zhu CH, et al. Contribution of mitophagy to cell-mediated mineralization: revisiting a 50-year-old conundrum. *Adv Sci*. 2018;5 (10):1800873. doi:10.1002/advs.201800873

59. Ma S, Li S, Zhang Y, et al. BMSC-derived exosomal CircHIPK3 promotes osteogenic differentiation of MC3T3-E1 cells via mitophagy. *Int J Mol Sci*. 2023;24(3): 2785.